

Performance of large chemically etched silicon grisms for infrared spectroscopy

D. J. Mar^{*a}, J. P. Marsh^a, D. T. Jaffe^a, L. D. Keller^b, K. A. Ennico^c

^aDept. of Astronomy C1400, Univ. of Texas at Austin, 1 University Station, Austin TX 78712

^bDept. of Physics, Ithaca College, 953 Danby Road, Ithaca, NY 14850

^cNASA-Ames Research Center, MS 245-6, Moffett Field, CA 94035

ABSTRACT

FORCAST is a mid/far-IR camera for use on NASA's SOFIA airborne observatory. We are fabricating monolithic silicon grisms to retrofit a spectroscopic capability for this facility-class instrument without affecting the imaging optics. The grisms will operate in the 5-8, 17-28, and 28-37 μm wavelength ranges. We will cover the 5-8 μm range in one exposure at a resolving power $R=1200$ with a 2 arcsecond slit using two grisms with one serving as a cross-disperser. For the 17-28 and 28-37 μm ranges, the resolving powers are $R\sim 140, 250$ when used in low order with a slit of 3 arcseconds. We illustrate aspects of fabrication and testing during the grism development, and summarize the performance of the gratings at near- and mid-IR wavelengths. These gratings rely on procedures that can be used for modest sized (~ 10 cm) silicon pieces, thereby providing dispersive elements with good optical performance and large slit width-resolving power products from 1.2-8.1 μm and beyond 17 μm .

Keywords: silicon, grism, infrared spectroscopy, FORCAST

1. INTRODUCTION

Studies of star formation and planetary system formation benefit from improvements in infrared spectroscopic capabilities at mid-infrared wavelengths (5-40 μm). This region contains spectral signatures from astrophysically relevant molecules (polycyclic aromatic hydrocarbons "PAHs", H_2O , CH_4 , and NH_3), as well as silicates important in the formation of disks around protostars. The airborne Stratospheric Observatory for Infrared Astronomy (SOFIA) [1], scheduled to begin operations in 2008, is equipped with a 2.5 m diameter infrared-optimized telescope and instruments designed to take advantage of operating altitudes (>40000 ft) above most of the telluric water vapor.

Table 1. List of silicon grisms for FORCAST and their design parameters. In Ref. 4, the parts are referred to by the numbers in the second column. The FORCAST grism complement contains two additional KRS-5 grisms (not listed here) that are intended for use at ~ 8.0 -13.7 μm . The physical parameters are the grating blaze angle (or wedge angle) δ , the groove spacing σ , and the groove top distance t . For a diagram of these dimensions, see Fig. 1. The expected resolving power for the given slit sizes in FORCAST is indicated in the last column.

grism	wavelength	optimized for		physical dimensions			resolving power	
		Ref. 4	λ [μm]	m	λ_{blaze} [μm]	δ [$^\circ$]		σ [μm]
G2	1	4.9 - 8.1	1	6.5	6.16	25	2.5	200 (with a 2" slit)
G3	2	4.9 - 8.1	14 - 23	4.9-8.1	32.6	87	6.0	1200 (G3 \times G2, 2" slit)
G4	5	17.1 - 28.1	1	22.4	6.16	87	6.0	140 (3" slit)
G5	6	28.6 - 37.4	2	32.7	11.07	142	10	250 (3" slit)

*djmar@astro.as.utexas.edu

One of the first-generation instruments on SOFIA is the Faint Object Infrared Camera for the SOFIA Telescope (FORCAST), a cryogenic (4 K) facility-class imager operating at $\lambda = 5\text{-}40\ \mu\text{m}$ [2,3]. Its first-light capabilities are limited to imaging, but by using reserve space in filter wheels for four silicon and two KRS-5 gratings [4], we can provide moderate resolution spectroscopic capabilities. The four silicon gratings, along with their physical design parameters (see Figure 1) and their corresponding expected resolving powers are listed in Table 1. We report on the fabrication techniques and bench-top performance of these gratings in the near-infrared, and summarize their current status here. In a companion paper in this volume [4] we report on their cryogenic performance within FORCAST.

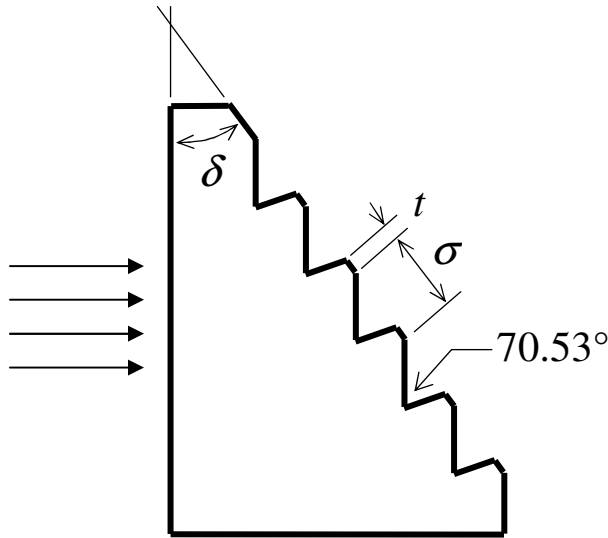


Figure 1. Schematic diagram of a silicon grating with wedge angle δ , groove spacing σ , and groove top t (an artifact of the fabrication process). The plane of the figure is a $\{110\}$ crystal plane and the groove facets are adjacent $\{111\}$ crystal planes. The vertical groove facet and the shorter unused facet meet at a valley angle of $\cos^{-1}(1/3) = 70.53^\circ$. Because the valley angle is not a right angle, and because of the presence of the groove tops, a geometric loss occurs where portions of the incident collimated beam (indicated in the figure by the arrows at left) must pass through the unused sloping facet and/or the groove top. When the groove facets are parallel to the entrance face, the blaze angle is equal to the wedge angle δ .

2. MATERIALS AND METHODS

2.1 Materials

Silicon is a desirable material from which to manufacture infrared gratings. High-resistivity silicon is transparent at wavelengths from ~ 1.2 to $6.6\ \mu\text{m}$ [5-7] and from ~ 25 to beyond $160\ \mu\text{m}$ [8]. Lattice absorption features occur from ~ 8 to $25\ \mu\text{m}$. By lowering the temperature to 77 K and below, some of this absorption can be suppressed [9]. In the range between ~ 9 and $\sim 17\ \mu\text{m}$, the absorption in the cooled silicon may be tolerable for path lengths up to a few mm, except for wavelengths around a particularly deep lattice absorption around $16\ \mu\text{m}$. Other absorption features due to oxygen impurities may occur near 9 and $19\ \mu\text{m}$ [7,10,11], but are generally not observed in high-resistivity float-zone silicon with low oxygen content. The resolving power of a grating is given by $R = \lambda/\Delta\lambda = (D/\lambda)(n - 1) \tan \delta$, where D is the diameter of the beam. When D is already fixed by the instrument design, the relatively high refractive index of silicon ($n \approx 3.38$ at 77 K) leads to large dispersion and high resolution, e.g., $R_{\text{Si}} \approx 1.7 R_{\text{KRS-5}}$.

Alternatives to silicon for the mid-IR include KRS-5, which has excellent optical transmission from 0.6 to $50\ \mu\text{m}$, without absorption features. Offsetting this advantage is the lower refractive index of KRS-5 ($n = 2.4$ at $\lambda = 1.5\ \mu\text{m}$ and $n = 2.2$ at $\lambda = 40\ \mu\text{m}$). It is also difficult to rule the deep ($\sim 100\ \mu\text{m}$) and coarse ($\sigma \sim 130\ \mu\text{m}$) grooves called for in the FORCAST grating complement, but these challenges appear surmountable [4] at $\lambda < 15\ \mu\text{m}$.

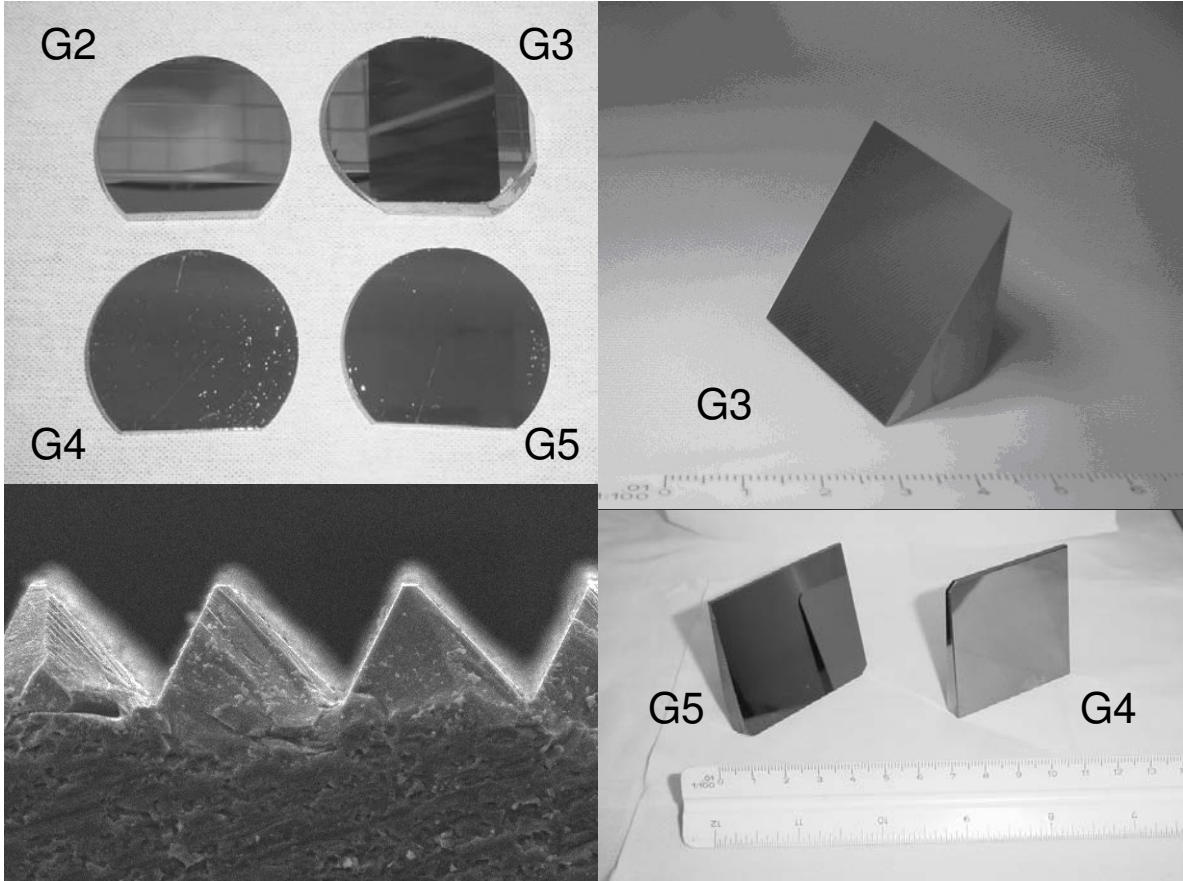


Figure 2. Images of silicon gratings taken after patterning and wet-etching. The upper left image shows the four gratings listed in Table 1 as etched into elliptical blanks, but before the devices have been shaped into prisms. The left-right direction is the dispersion direction. Reflections of the camera are visible in G2, and in the unetched areas of G3. The thicknesses of the blanks range from 9 mm to 15 mm. Images of complete grisms are shown in the right two images, with the ruled areas of G3 (37 mm × 32 mm), G4 (51 mm × 50 mm), and G5 (51 mm × 57 mm) shown towards the camera. These grisms all accommodate a 25 mm diameter beam, sufficient for use in FORCAST. The lower left image is a scanning electron microscope (SEM) scan of a grating with blaze angle 63.4° [30,31] and groove constant $\sigma = 80 \mu\text{m}$, showing the flatness of the grooves.

2.2 Grating Fabrication

The choice of silicon as a grating substrate material benefits from industrial microfabrication process technologies [12] that have been developed for semiconductor electronics and for micro-electro-mechanical systems applications. These technologies include lithographic processes [13] that can be used to pattern precisely positioned periodic lines in a thin mask layer that covers a silicon substrate. Anisotropic wet-etching through this mask forms aligned facets in the grating surface [14]. High etch anisotropy ratios produce periodic grooves that are flat, smooth, and aligned along the $\{111\}$ crystal planes.

A large amount of effort by the astronomical community has gone into the development of high quality diffraction gratings in Si [15-21]. Some of this work occurred using silicon wafers with a view towards mounting them on prism shaped Si or Ge substrates [22-24], and some have fabricated gratings on thick monolithic substrates [25-30], with the obvious advantage of avoiding potential optical and mechanical problems when bonding. Most work has focused on methods for producing gratings blazed at $\delta_{100} = \cos^{-1}(3^{-1/2}) = 54.7^\circ$, the natural angle that occurs for $\{100\}$ Si surfaces. Grism designs demand the flexibility to arbitrarily set the grism blaze angle over a wide range (e.g. see Table 1), a capability originally developed in [26] and extended in Ref. 30 and here. In our efforts at the University of Texas at

Austin [25,26,28,30] we have chosen to work with thick monolithic substrates, an approach that requires modifications to semiconductor processing technologies originally designed for working with thin wafer substrates. We have been successful in producing optical devices that are complete (see Fig. 2), except for commercial anti-reflection coatings.

To create the silicon grisms pictured in Fig. 2, we started from cylindrical ingots of high-purity monocrystalline float-zone silicon with resistivities in excess of 2000 ohm-cm. The crystal growth axis (e.g. $\langle 001 \rangle$ or $\langle 111 \rangle$) coincides with the cylinder axis to an accuracy of $\sim 1^\circ$. For a particular grism, the proper choice of growth axis depends on whether or not the desired blaze angle exceeds $\delta_{100}/2 = 27.4^\circ$. For blaze angles shallower than this value, starting from $\langle 001 \rangle$ material is preferable, since the resulting bias-slicing angle for $\langle 001 \rangle$ is smaller than that for $\langle 111 \rangle$ material and the eccentricity of the elliptical blanks is lower. Lower eccentricity blanks are easier to process since most semiconductor processing equipment is designed for circular wafers. Grisms G2, G4, and G5 ($\delta = 6.16, 6.16,$ and 11.07°) were produced from a single $\langle 001 \rangle$ ingot while G3 ($\delta = 32.6^\circ$) was produced from a separate $\langle 111 \rangle$ ingot. To set the blaze angle to an accuracy of 0.05° , and to prevent dislocations from appearing during the wet-etch micromachining process that creates the long grooves, the ingot is oriented by using x-ray diffractometry to locate the crystal directions within the ingot to an accuracy of $0.03\text{-}0.04^\circ$. A precision $\{110\}$ flat is then ground onto one side of the ingot. This flat serves as a stable mount for cutting and in later lithography steps it is a precise alignment marker. The ingot is then sliced into elliptical blanks (see upper left panel in Fig. 2) and the fresh surfaces are ground, etched to relieve saw damage, and polished flat to surface figures less than $1/50$ wave rms at 632.8 nm. The polishing is done by chemical-mechanical planarization (CMP), which results in less mechanical stress at and near the surface. The blanks are then coated with a $\sim 100 \pm 5$ nm uniform layer of low pressure chemical vapor deposition (LPCVD) silicon nitride as a passivation layer.

The next steps in the fabrication use ultraviolet photolithography to create a series of precisely positioned periodic array of lines in the silicon nitride, and a KOH-water-isopropanol wet-etch to chemically micromachine grooves into the silicon surface. These steps involve custom-built or modified equipment (spin table, UV mask contact aligner, and a plasma etcher) that can accommodate bulky elliptical blanks with thicknesses up to ~ 35 mm. Details of these steps are described elsewhere [25,27,28,30,31]. After washing the blanks in hot (150°C) phosphoric acid to remove residual silicon nitride, the gratings reach the state shown in the upper left panel of Fig. 2.

The devices are shaped into wedges and the flat entrance faces opposite the grating sides are polished flat to surface figures less than $1/20$ wave rms at 632.8 nm across a 25 mm circular aperture or greater (grisms G2, G4, and G5 are large enough to accommodate a 35 mm diameter beam). For the devices shown in Fig. 2, the entrance faces are formed parallel to the grating facets. Except for anti-reflection coatings that can be applied to the entrance and grating surfaces, grisms G3, G4, and G5 are now essentially complete. Grism G2 has not yet been cut to the desired prism shape.

3. EVALUATION

3.1 Optical evaluations

Before integrating these grisms into FORCAST, we evaluated their performance by a number of bench-top optical measurements at visible and infrared wavelengths. In Figure 3, we show transmission spectra for grisms G3, G4, and G5. Collimated light from a 1523 nm HeNe laser is used to illuminate the entrance face of the grisms, and the diffracted beams are focused with a $f = 125$ mm lens onto a Alpha NIR InGaAs array ($0.9\text{-}1.7$ μm , 320×256 format, 30 μm pixels). In our setup, the beam diameter is limited to 10 mm by the infrared collimator optics. The laser wavelength is not on the blaze for these grisms, so that each spectrum appears as an array of orders. For each grism, we obtain an estimate of the throughput efficiency by summing up the power in the series of diffracted orders and comparing the total to the power measured in the incident beam. The result is approximately equal to the power one would observe in a single order for a laser at the blaze wavelength. In Table 2, we list these measured efficiencies for the uncoated grisms. These values should be compared to the transmission for a beam that suffers reflective Fresnel losses of $(n - 1)^2/(n + 1)^2$ at each of the Si/air interfaces (49% transmission for a device with two surfaces). As a better indicator of actual performance, the table lists the throughput expected when the grisms have been equipped with broadband anti-reflection (BBAR) coatings. The expected throughput values assume that each coating surface causes a 5% loss. The somewhat lower throughput values for G3 (measured $T = 31\%$, uncoated) result from geometric losses where the beam area is partially obscured by the groove top and the unused facet (see Fig. 1).

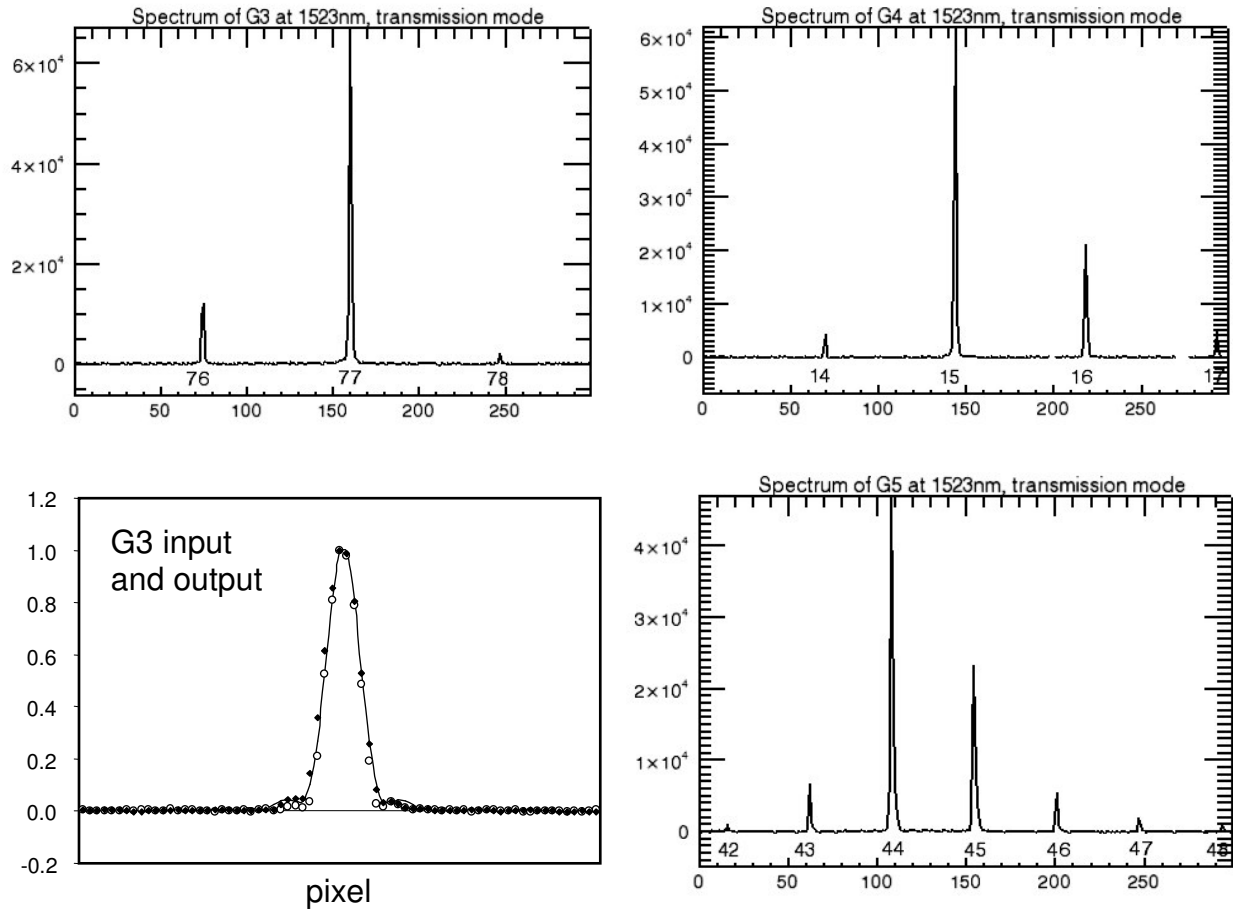


Figure 3. Transmission spectra of gratings G3 (upper left), G4 (upper right), and G5 (lower right), obtained by illuminating each grating using a 10 mm diameter collimated beam at $\lambda = 1523$ nm. Order numbers are indicated at the bottom of each peak. The lower left plot is a normalized one-dimensional point spread function (PSF) for the same beam, obtained using a slower camera. With this optical setup the FWHM of the PSF corresponds to $R = 1 \times 10^4$. Filled symbols show the transmission PSF measured for silicon grating G3. It is a magnification of the brightest diffraction order shown in the upper left plot. The horizontal axis is the dispersion direction. Open symbols show the corresponding data taken for the incident beam alone. Both sets of symbols nearly coincide with the theoretical curve (solid line) computed for a 10 mm diameter circular aperture, indicating diffraction-limited performance over this beam. Before normalizing, the peak value of the grating PSF was 48% of that measured for the incident beam, as expected for nearly perfect transmission through two uncoated Si ($n = 3.4$) surfaces.

Table 2. Efficiencies for the three gratings shown in the right two panels of Fig. 2. The measured transmission is taken using a 10 mm collimated beam at $\lambda = 1523$ nm. The estimates given in the final column for the efficiency on the blaze assume that the Fresnel losses at the uncoated Si-air interfaces are reduced by the use of BBAR coatings with 5% loss.

grating	design aperture (mm)	measured T (%) 10 mm beam, 1523 nm	estimated T (%) with 2 sides BBAR @ 5% loss
G3	23	31	57
G4	25	44	81
G5	25	48	88

In the lower left panel of Fig. 3 we show a one-dimensional point-spread function (PSF) taken in transmission at $\lambda = 1523$ nm. The optical setup is similar to that for the three other plots in Fig. 3, except that the focusing lens is slower ($f = 838$ mm). Two-dimensional images of the brightest diffraction order are collected and collapsed in the cross-spectral direction to form the one-dimensional PSF shown for grism G3. Overlaid on the same plot are data for the incident beam and the theoretical curve for a circular aperture. The close agreement between the data sets and the theoretical curve demonstrate that the grism has diffraction-limited performance over the 10 mm aperture, even at near-infrared wavelengths. The width of the spectral PSF for this input beam size corresponds to $R = \lambda/\Delta\lambda = 1 \times 10^4$. Before normalization, the peak value of the grism output PSF was 48% that of the incident beam, a measurement consistent with the expected Fresnel losses of $[4n/(n + 1)]^2 = 49\%$ for two air-silicon interfaces.

External reflection measurements are also useful to assess the quality of the gratings. In Fig. 4 we show surface error plots of the grating surfaces, based on interferograms taken in reflection using red HeNe light at $\lambda = 632.8$ nm. While the efficiency and PSF measurements above test the grating over a 10 mm aperture, these interferometric results assess the full 25 mm aperture required for FORCAST. As shown in Fig. 4, the residual errors are small and correlated into structures with long (several mm or more) spatial wavelengths. The surface figures are excellent ($\lambda/100$, $\lambda/100$, $\lambda/38$, and $\lambda/32$). The grating quality is evident even at wavelengths in the visible. Since the infrared application wavelengths are all at least seven times λ , the performance of the gratings greatly exceeds that required for FORCAST. It should be noted that the data in Fig. 4 were taken after etching but before the devices were shaped into final prisms (see upper left panel in Fig. 2). We have verified that as long as the parts are reasonably thick (several mm), forming the entrance face and polishing it to optical flatness ($\lambda/20$) does not degrade the surface figure of the grating.

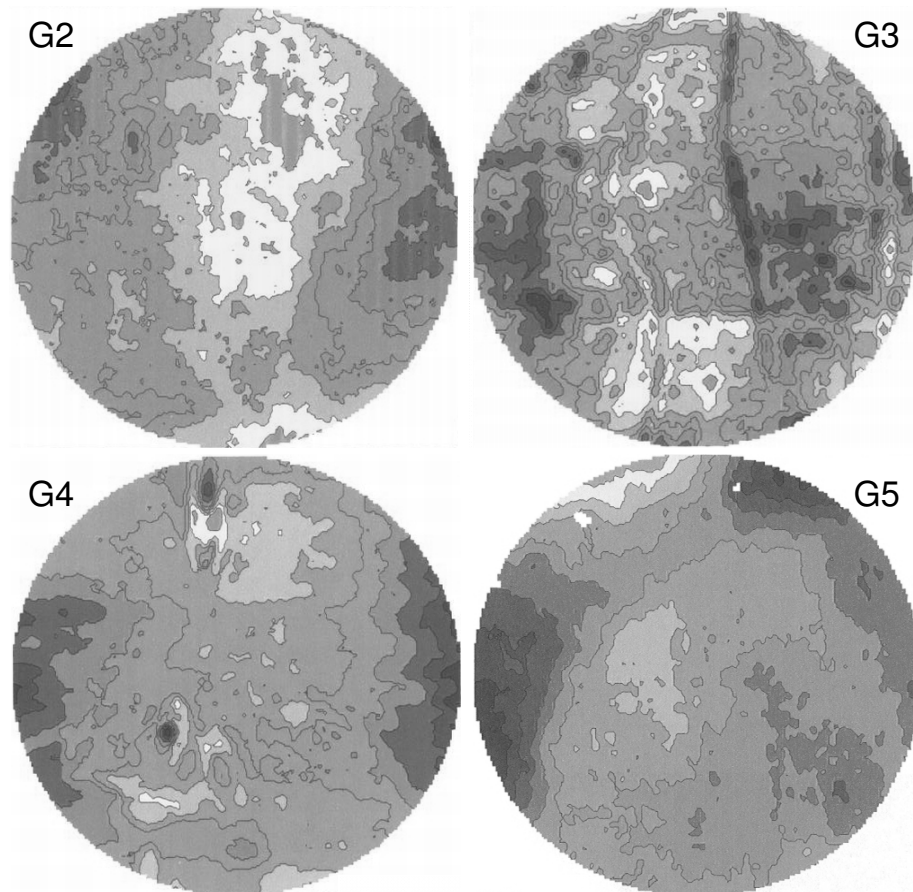


Figure 4. Surface error plot of the gratings measured using a Zygo interferometer using laser light at $\lambda = 632.8$ nm. Each circle is a 25 mm aperture. Contours correspond to $\lambda/154$, $\lambda/157$, $\lambda/50$, and $\lambda/42$ in the four plots. The rms surface figures of these are $\lambda/100$, $\lambda/100$, $\lambda/38$, and $\lambda/32$. These data were taken before the gratings were shaped into gratings.

3.2 Physical evaluations

To complement the optical performance measurements in Section 3.1, we use a battery of physical probes such as scanning electron microscopy (SEM), surface profilometry, and atomic force microscopy (AFM). Scanning electron microscope images (see lower left panel of Fig. 2) are useful for discovering and evaluating defects on the surface, and verifying that the grating surfaces are smooth and flat. However, from SEM images alone, it is difficult to accurately measure the blaze and valley angles of the grating, because small tilts can confound the interpretation of images. Surface profilometry can be used to accurately measure the slopes of the groove facets. Using a Veeco Dektak 6M profilometer, and calibrating for stylus arm arcing, for our gratings we measure a valley angle of 72.12° with a measurement uncertainty of less than 0.05° , close to the theoretical value of $\cos^{-1}(1/3) = 70.53^\circ$ formed by the intersection of adjacent families of $\{111\}$ crystal planes in the silicon. The difference reflects a finite anisotropy ratio of the etch rates between the $\langle 111 \rangle$ and $\langle 001 \rangle$ directions and it leads to a global tilt of the grating facets and consequently, a small 0.8° shift in the blaze angle δ from the design value. When orienting silicon crystal for new devices, this anisotropy shift should be taken into account.

Atomic force microscopy (AFM) scans are useful for measuring the surface roughness of the individual facets. Excessive roughness is undesirable because it can lead to diffuse scattered light. As shown in Fig. 5, the surface roughness of our etched silicon facets is very small, approximately 1.5 nm rms. By scanning different regions across the facet, we have verified that the roughness is unchanged across the entire facet. Taken together, the AFM, SEM, and profilometer scans demonstrate that individual grooves are smooth and flat. These scans complement optical measurements (Figs. 3 and 4) that assess the accuracy and precision of groove placement.

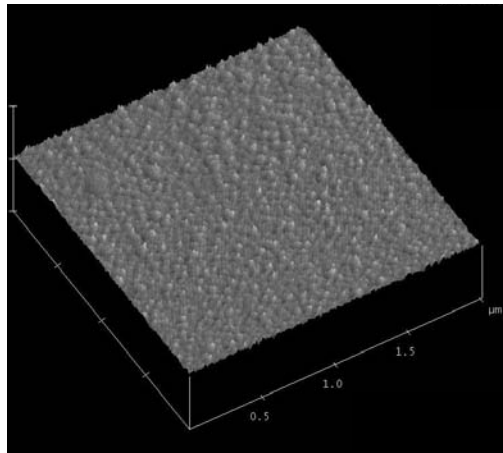


Figure 5. Surface of a groove facet obtained using an atomic force microscope (AFM). The field measures $2 \mu\text{m} \times 2 \mu\text{m}$, and the surface roughness over this area is measured to be approximately 1.5 nm rms. The scan is taken from an offcut of grism G2.

4. STATUS

As shown in the previous Section, the gratings are clearly of science-grade quality and their optical performance exceeds requirements for applications in the mid-infrared. The quality of these gratings and others developed for immersion grating applications [30] are sufficient even for use in the near-infrared ($1\text{-}5 \mu\text{m}$). We have shown a resolving power $R = 1 \times 10^4$ for grism G3 used in transmission, and, from additional surface figure reflection measurements, infer a value of $R = 2.5 \times 10^4$ across a 25 mm beam. We are continuing to develop procedures to fabricate devices with larger apertures and better overall performance. Even so, the silicon grism devices described here demonstrate that the technology of manufacturing silicon diffractive optics has matured to the point where these devices find profitable use in near and mid-infrared spectrographs for astronomy.

Three of the four silicon grisms (G3, G4, G5) in the FORCAST grism suite are essentially complete except for the application of broadband anti-reflection (BBAR) coatings to optimize the infrared throughput in the appropriate wavelength bands. The remaining grism (G2) was miscut and will have to be remade, and finally coated. This is not expected to be problematic, and spare silicon blanks of the appropriate orientation are in hand.

4.1 Anti-reflection coatings

We have contracted with commercial vendors to develop the challenging mid-infrared BBAR coatings required for these grisms. In the left panel of Fig. 6 we show the performance of the baseline 4.8-8.1 μm coating design, suitable for grisms G2 and G3. As shown, the throughput exceeds 66% across the specified wavelength region, indicating that the one-surface transmission is around 95%. This coating has been successfully applied to planar and grating surfaces of silicon witnesses, with excellent uniformity (see the right panel of Fig. 6), durability, and cryogenic performance. This coating adheres well even under multiple rapid (few sec) thermal cyclings between room temperature and 77 K.

The coatings for G4 and G5 have not been developed as extensively. A test coating with adequate (90%) one-pass performance from 17.5 to 26.9 μm has been developed for G4, although some further work will be needed to fully cover the original wavelength range specification for G4 (17.1-28.1 μm) and possibly to extend its range to cover that for G5 (to 37.4 μm) as well. Since this coating is relatively thick and may contain internal stresses, it will be important to assess its durability, especially during thermal cooldowns, when it is applied to corrugated grating surfaces. The resistance of the coating to humid environments should also be checked.

4.2 Integration

Although uncoated, grism G4 has been mounted and tested within FORCAST at Cornell University. Preliminary results of these tests verify that despite the Fresnel losses that limit the maximum throughput, the grism performs well ($R \sim 150$, 17-28 μm). Results of these tests are described in Ref. 4.

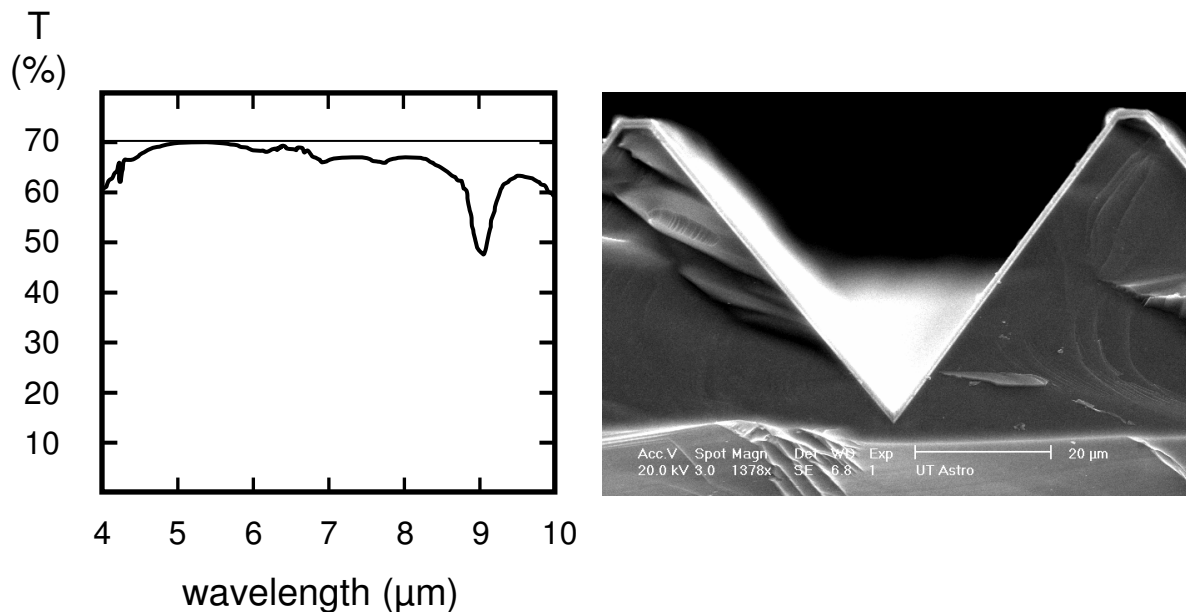


Figure 6. (left) One-pass transmission of a 4.8-8.1 μm broadband anti-reflection coating applied to one face of a 1 mm thick silicon witness. The dip at 9 μm is likely due to the presence of oxygen in the witness. The horizontal line at 70% shows the maximum transmission expected for a silicon part with one side coated and the other side uncoated. This BBAR coating has also been successfully applied to a silicon grating surface. In the SEM micrograph at (right) the coating is visible as a bright layer covering the groove surfaces and groove tops of a symmetric ($\delta = \delta_{100} = 54.7^\circ$) grating. The coverage is smooth and uniform.

4.3 Acknowledgements

This work is supported by NASA grants NAG5-8858, NRA 03-OSS-01 via the Astrobiology Science and Instrument Development (ASTID) program, and NNA 05CS83A via the NASA Astrobiology Institute (NAI), and by funding from the Universities Space Research Association (USRA 8500-98-008), the Welch Foundation, and McDonald Observatory at the University of Texas at Austin. Fabrication and testing of the grisms and other silicon gratings were made possible by facilities at the University of Texas at Austin, including the Center for Nano and Molecular Science and Technology (CNM) and the Microelectronics Research Center (MRC), funded in part by the National Science Foundation through the National Nanotechnology Infrastructure Network (NNIN). We thank R. Joyce, K. Hinkle, and G. Poczulp of NOAO for Zygo measurements. We thank K. Allers and S. Joshi for assistance in process development, and T. Gaubert and W. Frey for help with AFM measurements.

REFERENCES

1. E. F. Erickson and J. A. Davidson, "SOFIA: The future of airborne astronomy", in *Airborne Astronomy Symposium on the Galactic Ecosystem: From Gas to Stars to Dust, ASP Conference Series*, **73**, 707-773 (1995).
2. L. D. Keller, T. L. Herter, G. J. Stacey, G. E. Gull, J. Schoenwald, B. Pirger, and T. Nikola, "FORCAST: the faint object infrared camera for the SOFIA telescope", *Proc. SPIE* **4857**, 29-36 (2003).
3. J. D. Adams, T. L. Herter, L. D. Keller, G. E. Gull, B. E. Pirger, J. Schoenwald, M. Berthoud, G. J. Stacey, and T. Nikola, "FORCAST: the facility mid-infrared camera for SOFIA", *Proc. SPIE*, this volume.
4. K. A. Ennico, L. D. Keller, D. J. Mar, T. L. Herter, D. T. Jaffe, J. D. Adams, and T. P. Greene, "Grism performance for mid-infrared (5-40 micron) spectroscopy", *Proc. SPIE*, this volume.
5. H. Y. Fan and M. Becker, "Infra-Red Absorption of Silicon", *Phys. Rev.* **78**, 178-179 (1950).
6. W. Spitzer and H. Y. Fan, "Infrared Absorption in n-Type Silicon", *Phys. Rev.* **108**, 268-271 (1957).
7. W. R. Runyan, *Silicon Semiconductor Technology*, McGraw-Hill, New York (1965).
8. J. E. Peters and P. D. Ownby, "Far-infrared transmission of diamond structure semiconductor single crystals--silicon and germanium", *Opt. Eng.* **38**, 1924-1931 (1999).
9. W. C. Dash and R. Newman, "Intrinsic Optical Absorption in Single-Crystal Germanium and Silicon at 77°K and 300°K", *Phys. Rev.* **99**, 1151-1155 (1955).
10. W. Kaiser, P. H. Keck, and C. F. Lange, "Infrared Absorption and Oxygen Content in Silicon and Germanium", *Phys. Rev.* **101**, 1264-1268 (1956).
11. H. J. Hrostowski and R. H. Kaiser, "Infrared Absorption of Oxygen in Silicon", *Phys. Rev.* **107**, 966-972 (1957).
12. M. J. Madou, *Fundamentals of Microfabrication*, CRC Press, Boca Raton (1997).
13. M. J. Bowden, "The Lithographic Process: The Physics", in *Introduction to Microlithography, 2nd ed.*, edited by L. F. Thompson, C. G. Willson, and M. J. Bowden, American Chemical Society, Washington (1994).
14. W. T. Tsang and S. Wang, "Preferentially etched diffraction gratings in silicon", *J. Appl. Phys.* **46**, 2163-2166 (1975).
15. G. Wiedemann and D. E. Jennings, "Immersion grating for infrared astronomy", *Appl. Optics* **32**, 1176-1178 (1993).
16. P. J. Kuzmenko, D. R. Ciarlo, and C. G. Stevens, "Fabrication and testing of a silicon immersion grating for infrared astronomy", *Proc. SPIE* **2266**, 566-577 (1994).
17. P. J. Kuzmenko and D. R. Ciarlo, "Improving the optical performance of etched silicon gratings", *Proc. SPIE* **3354**, 357-367 (1998).
18. U. U. Graf, D. T. Jaffe, E. J. Kim, J. H. Lacy, H. Ling, J. T. Moore and G. Rebeiz, "Fabrication and evaluation of an etched infrared diffraction grating", *Appl. Optics* **33**, 96-102 (1994).
19. L. D. Keller, D. T. Jaffe, O. A. Ershov, T. Benedict, and U. U. Graf, "Fabrication and testing of chemically micromachined silicon echelle gratings", *Appl. Optics* **39**, 1094-1105 (2000).
20. D. T. Jaffe, L. D. Keller, and O. Ershov, "Micromachined silicon diffraction gratings for infrared spectroscopy", *Proc. SPIE* **3354**, 201-212 (1998).
21. J. Ge, D. Ciarlo, P. Kuzmenko, B. Macintosh, C. Alcock, and K. Cook, "Etched Silicon Gratings for NGST", in *Proc. Next Generation Space Telescope Science and Technology, ASP Conference Series* **207**, 457-461, (2000).
22. H. U. Käüfl, K. Köhl, and S. Vogel, "Grisms from Germanium/Silicon for Astronomical Instruments", *Proc. SPIE* **3354**, 151-158 (1998).

23. F. Vitali, E. Cianci, D. Lorenzetti, V. Foglietti, A. Notargiacomo, E. Giovine, and E. Oliva, "Silicon grisms for high-resolution spectroscopy in the near infrared", *Proc. SPIE* **4008**, 1383-1394 (2000).
24. F. Vitali, E. Cianci, V. Foglietti, and D. Lorenzetti, "Fabrication of silicon grisms", *Proc. SPIE* **4842**, 274-281 (2003).
25. O. A. Ershov, D. T. Jaffe, J. P. Marsh, and L. D. Keller, "Production of high-order micromachined silicon echelles on optically flat substrates", *Proc. SPIE* **4440**, 301-308 (2001).
26. O. A. Ershov, J. P. Marsh, K. N. Allers, and D. T. Jaffe, "Infrared grisms using anisotropic etching of silicon to produce a highly asymmetric groove profile", *Proc. SPIE* **4850**, 805-812 (2003).
27. J. Ge, D. L. McDavitt, S. Miller, J. L. Bernecker, A. Chakraborty, and J. Wang, "Breakthroughs in silicon grism and immersion grating technology at Penn State", *Proc. SPIE* **4841**, 1006-1015 (2003).
28. J. P. Marsh, O. A. Ershov, and D. T. Jaffe, "Silicon grisms and immersion gratings produced by anisotropic etching: testing and analysis", *Proc. SPIE* **4850**, 797-804 (2003).
29. D. L. McDavitt, J. Ge, S. Miller, and J. Wang, "Silicon immersion gratings for very high-resolution infrared spectroscopy", *Proc. SPIE* **5494**, 536-544 (2004).
30. J. P. Marsh, D. J. Mar, and D. T. Jaffe, "Fabrication and performance of silicon immersion gratings for infrared spectroscopy", *Proc. SPIE*, this volume.
31. J. P. Marsh, "Production and Evaluation of Silicon Diffractive Optics for Infrared Astronomy", Ph.D. dissertation, The University of Texas at Austin, (2006).